nature climate change

LETTERS

PUBLISHED ONLINE: 10 AUGUST 2015 | DOI: 10.1038/NCLIMATE2758

Shift from coral to macroalgae dominance on a volcanically acidified reef

I. C. Enochs[1,2]*, D. P. Manzello[2], E. M. Donham[3,4], G. Kolodziej[1,2], R. Okano[5], L. Johnston[5], C. Young[6], J. Iguel[5], C. B. Edwards[7], M. D. Fox[7], L. Valentino[1,2], S. Johnson[5], D. Benavente[5], S. J. Clark[6], R. Carlton[1,2], T. Burton[1], Y. Eynaud[7] and N. N. Price[4]

Rising anthropogenic CO_2 in the atmosphere is accompanied by an increase in oceanic CO_2 and a concomitant decline in seawater pH (ref. 1). This phenomenon, known as ocean acidification (OA), has been experimentally shown to impact the biology and ecology of numerous animals and plants[2], most notably those that precipitate calcium carbonate skeletons, such as reef-building corals[3]. Volcanically acidified water at Maug, Commonwealth of the Northern Mariana Islands (CNMI) is equivalent to near-future predictions for what coral reef ecosystems will experience worldwide due to OA. We provide the first chemical and ecological assessment of this unique site and show that acidification-related stress significantly influences the abundance and diversity of coral reef taxa, leading to the often-predicted shift from a coral to an algae-dominated state[4,5]. This study provides field evidence that acidification can lead to macroalgae dominance on reefs.

Coral reefs contain the highest concentration of biodiversity in the marine realm, with abundant flora and fauna that form the backbone of complex and dynamic ecosystems[6]. From an anthropocentric standpoint, coral reefs provide valuable goods and services, supporting fisheries and tourism, and protect shorelines from storms[7]. Recently, widespread coral mortality has led to the flattening of reef frameworks and the loss of essential habitat[4]. This trend will be accelerated by ocean acidification (OA), as calcification is impaired, and dissolution is accelerated[8,9]. Furthermore, experimental evidence suggests that OA could enhance the growth[10] and competitive ability of fleshy macroalgae[11]. This OA-induced shift in the competitive balance between corals and algae could exacerbate direct effects of OA on calcifying reef species[12] and lead to ecosystem shifts favouring non-reef-forming algae over coral[4,5]. Understanding the individual responses of taxa to OA, as well as alteration of multi-species assemblages, is therefore critical to predicting ecosystem persistence and managing reef health in an era of global change.

At present, much of what is known concerning the impacts of OA on coral reef biota has been laboratory-based experimental work focused on the responses of select taxa[2]. This has been expanded to mesocosm-based studies, allowing manipulation of groups of organisms and investigation of community responses[13]. Although these multi-species experimental studies are vital, they cannot recreate the variability (physical, chemical, biological) of real-world reef systems[14]. In an effort to overcome the limitations of laboratory studies, real-world low-saturation-state (Ω) sites have been investigated. In the eastern Pacific, nutrient and CO_2-enriched upwelled waters impact coral calcification and the precipitation of carbonate cements, influencing the distribution of reefs[15]. In Mexico, freshwater springs depress Ω, influencing coral calcification and species distributions[16]. In Palau, restricted circulation and biological activity contribute to elevated p_{CO_2}, with little impact on reef communities[17]. These locations provide insight into community-scale responses to OA; however, variation in other environmental parameters can complicate conclusions.

Volcanic enrichment of CO_2 from submarine vents has been shown to impact the structure of temperate and sub-tropical ecosystems, including seagrasses[18], rocky-shore and rocky-reef communities[19,20], soft sediments[21] and vermetid reefs[22]. The occurrence of CO_2 vents near coral reef ecosystems is rare and, at present, only two regions have been studied: Papua New Guinea (PNG; ref. 23) and a sub-tropical system at Iwotorishima Island, Japan[24]. High-p_{CO_2} vent communities in Japan, comparable to conditions projected for the end of the century (pH $\approx$ 7.8) are dominated by soft corals, whereas nearby control sites (pH $\approx$ 8.1) are dominated by hard scleractinian corals[24]. In PNG, coral cover is not significantly different at a pH of 7.8, although species composition changes and diversity is reduced[23]. Given the different ecosystem responses observed at the previously described sites and the paucity of temporally and spatially explicit data sets, further work is necessary to examine the multifarious influences of OA on coral reefs.

Here we identify and characterize a CO_2 vent impacting a tropical coral reef ecosystem in the Commonwealth of the Northern Mariana Islands (CNMI; Fig. 1). We use high-accuracy instrumentation to characterize the carbonate chemistry of this system and investigate its relationship with reef community composition (Methods).

Bubbling of subterranean gas was observed along the inner margin of the eastern side of the caldera. The spatial gradient in carbonate chemistry was investigated using 33 discrete water samples spaced over the study site. Samples were analysed for dissolved inorganic carbon (DIC) and total alkalinity (TA), and were

[1]Cooperative Institute for Marine and Atmospheric Studies, Rosenstiel School of Marine and Atmospheric Science, University of Miami, 4600 Rickenbacker Causeway, Miami, Florida 33149, USA. [2]Atlantic Oceanographic and Meteorological Laboratories (AOML), NOAA, 4301 Rickenbacker Causeway, Miami, Florida 33149, USA. [3]Moss Landing Marine Laboratories, 8272 Moss Landing Road, Moss Landing, California 95039, USA. [4]Bigelow Laboratory for Ocean Sciences, 60 Bigelow Drive, East Boothbay, Maine 04544, USA. [5]CNMI Bureau of Environmental and Coastal Quality, Division of Coastal Resources Management, Gualo Rai Center Chalan Pale Arnold, Middle Road, Saipan, Northern Mariana Islands 96950, USA. [6]Joint Institute for Marine and Atmospheric Research (JIMAR), NOAA/University of Hawaii, 1000 Pope Road, Marine Science Building 312, Honolulu, Hawaii 96822, USA. [7]Center for Marine Biodiversity and Conservation, Scripps Institution of Oceanography, University of California, San Diego, 9500 Gilman Drive, La Jolla, California 92093, USA. *e-mail: ienochs@rsmas.miami.edu

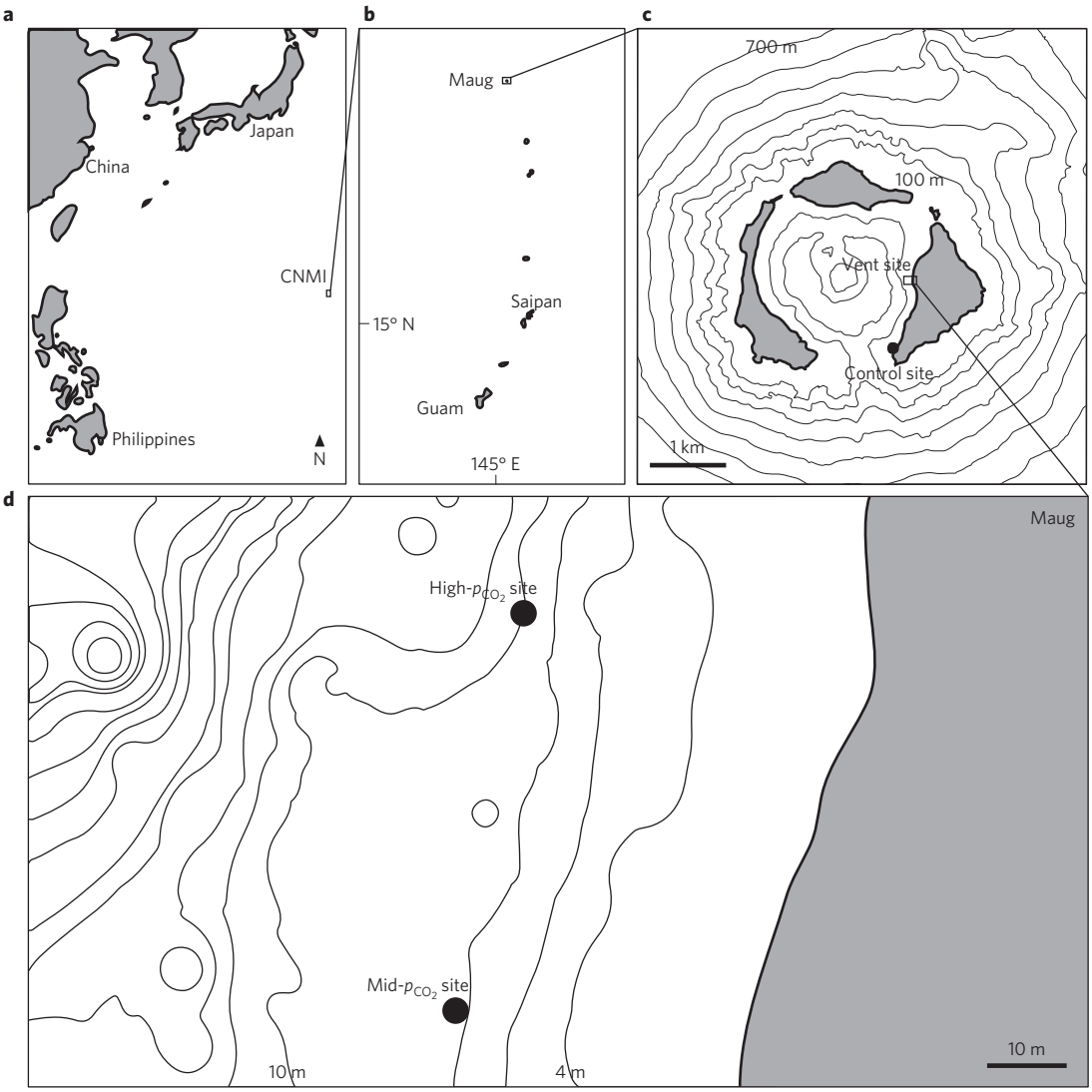

Figure 1 | Map showing the location of the study site at Maug. a, Location of the Commonwealth of the Northern Mariana Islands (CNMI). **b**, Location of Maug. **c**, The three main islands of Maug, with 100 m isobaths and the location of both the vent and control sites. **d**, Detail of the vent with the high-p_{CO_2} and mid-p_{CO_2} study sites, together with 2 m isobaths.

subsequently interpolated with ArcGIS. The resulting snapshot of the carbonate chemistry revealed a localized depression of pH and Ω (Fig. 2). The gradient extended over a distance >150 m from the centre of active bubbling and encompassed habitat with living corals and reef framework. This gradient was a result of enrichment of DIC versus TA, as the increase in DIC (634 μmol kg^{-1}) was more than an order of magnitude greater than the maximum change in alkalinity (54 μequiv. kg^{-1}). The CO_2 dynamics of Maug are similar to the vents in PNG (ref. 23), where plume attenuation is over comparable spatial scales. Furthermore, the ambient-CO_2 control site at Iwotorishima was located approximately 200 m from the zone of active bubbling, suggesting similar depletion of the vent signal[24].

Three sites of similar depth (~9 m) were selected for analysis of temporal fluctuation in environmental parameters, a high-p_{CO_2} site, mid-p_{CO_2} site and a control site roughly 1 km south of the vent. Shallow areas of extreme bubbling and carbonate undersaturation were avoided to investigate realistic OA scenarios and limit potentially confounding factors. A three-month deployment of SeaFET pH sensors at the three study sites revealed a dynamic gradient in seawater carbonate chemistry (Fig. 2e). Mean pH (± s.d.) was lowest at the high-p_{CO_2} site (7.94 ± 0.051, Min = 7.72), followed by the mid-p_{CO_2} (7.98 ± 0.027, Min = 7.76) and the control (8.04 ± 0.016, Min = 7.98) sites (Supplementary Table 1). Bottle samples taken over 48 h indicate that the diel oscillation in pH observed at all sites is due to changes in DIC, rather than TA (Supplementary Fig. 1). The diurnal amplitude in pH at the mid-p_{CO_2} site was greater than the control site. This is most likely a result of the nearness of the mid-p_{CO_2} site to the vent, as the pattern of variability in DIC was similar to the high-p_{CO_2} site. Although some day/night fluctuation is evident at the high-p_{CO_2} site, the majority of variation in seawater acidity occurs over longer periods, suggesting control by vent gas production.

Two one-month time series from vents in the Mediterranean show similar temporal variability in pH, although much lower pH was recorded at the near-vent site[12]. Higher CO_2 sites exhibited greater day-to-day fluctuation and a greater magnitude in diel oscillation than control sites[12]. Although day-to-day variability is difficult to discern from the four-day simultaneous deployment of pH loggers at Iwotorishima, higher diel fluctuation is again apparent at the vent versus control sites[24]. This temporal variability is important to investigate further.

Gas chromatography of vent gas samples showed high concentrations of CO_2 and relatively low concentrations of methane

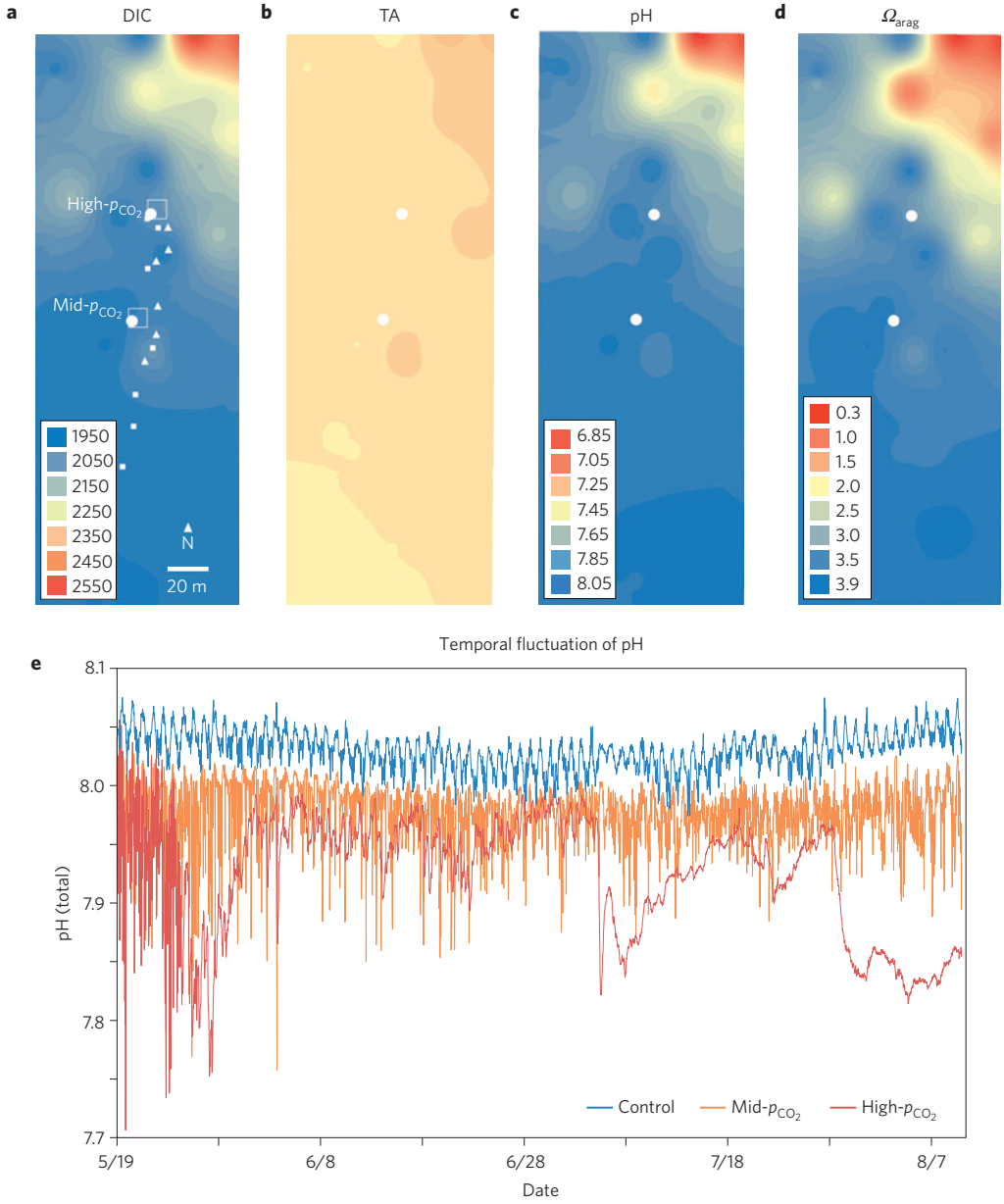

Figure 2 | Spatial extent of the acidified vent plume and location of sites as determined by interpolation of single-point bottle sample data ($n = 33$). **a**,**b**, Dissolved inorganic carbon (DIC, μmol kg^{-1}) (**a**) and total alkalinity (TA, μequiv. kg^{-1}) (**b**), presented on the same colour scale. **c**, $pH_{(total)}$. **d**, Aragonite saturation state (Ω_{arag}). **e**, Time-series pH data at the high-CO_2, mid-CO_2 and control sites. Open rectangles in **a** show the approximate locations of the photo mosaics. SeaFETs were deployed at the large closed circles. The location of benthic cover and *in situ* richness transects are denoted with small closed squares and triangles, respectively. The carbonate chemistry presented in **a**–**d** represents a single snapshot of conditions and should not be interpreted as the static conditions present in each transect, given the variability in the time-series data shown in **e**.

and sulphur compounds (Supplementary Table 2). Although other environmental parameters were found to differ between sites (Supplementary Fig. 2 and Supplementary Table 1), we do not expect these to be major drivers of benthic community structure. For instance, reduction of photosynthetically active radiation (PAR), associated with light attenuation with depth, was not correlated with changes in coral cover outside of the vent plume. In fact, deeper, lower-light waters along the slope of the caldera had higher coral cover than in better-illuminated shallow waters. Differences in mean temperature and flow between the high-p_{CO_2} and control sites were probably too small ($\Delta 0.2\,^{\circ}C$, $\Delta 0.03\,m\,s^{-1}$) to influence the shift from coral to macroalgal dominance. Regardless, it is well established that lower light may reduce coral calcification[25], high temperatures can lead to mortality[26], and high flow can enhance macroalgae growth[27]. The covariance of these factors therefore cannot be completely disregarded.

We observed a clear shift from coral to a fleshy macroalgae ecosystem at low pH (Figs 3 and 4 and Supplementary Tables 3 and 4). The dominant alga at the high-p_{CO_2} site was *Spatoglossum stipitatum*, covering >50% of the substrate in the high-p_{CO_2} photomosaic. This species, however, was not common in the richness transects that were placed at incrementally greater distances just outside of the zone of active bubbling. This shift in percentage cover is accompanied by a decrease in coral diversity approaching the high-CO_2 site and a drop in calcifying algae richness (Supplementary Fig. 3 and Supplementary Table 4). The pH-associated change in ecosystem state is probably due to multiple factors, including CO_2-depressed calcification[3]. This is apparent

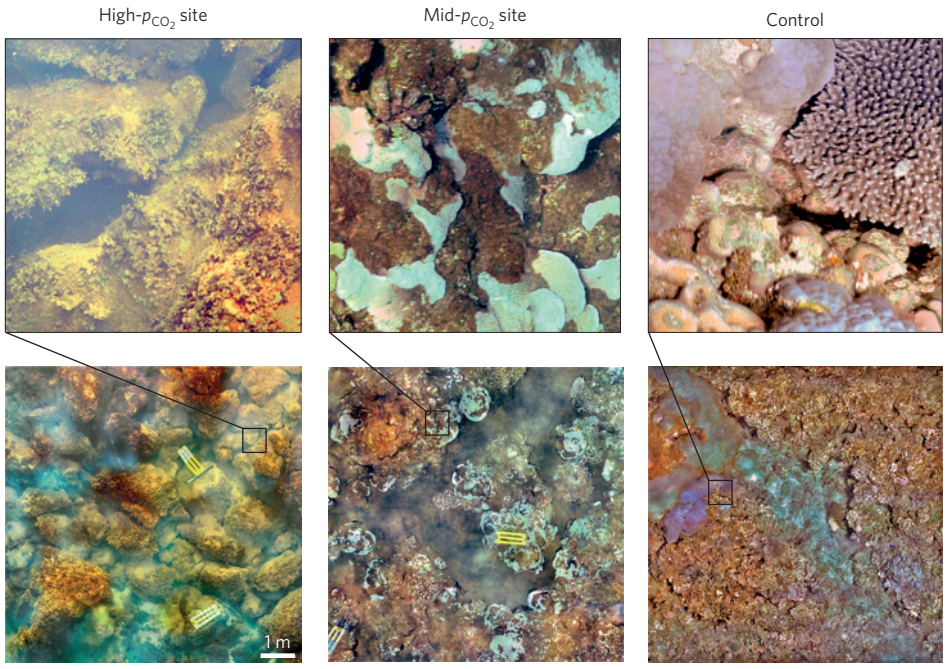

Figure 3 | High-resolution photomosaic imagery of benthic cover at high-p_{CO_2}, mid-p_{CO_2} and control sites, showing the progression from coral-dominated to algae-dominated systems. Top images are details of the selected region in the photomosaic below.

in the reduced calcification rates of relatively resilient[23] massive *Porites* (Supplementary Fig. 4 and Supplementary Tables 5 and 6), which were determined from coral cores following ref. 15. These findings support previous experimental[28] and field-based work[15], but represent the first evidence of this response on a volcanically acidified reef. Contrary to our findings, the percentage cover of massive *Porites* at the PNG vent sites was higher in lower-pH waters, with the exception of extremely active vents where pH was less than 7.7 (ref. 23). As with this study, growth records at PNG were produced from analysis of coral cores but, in contrast to our data, they revealed similar calcification rates across pH gradients[23]. It is unclear why calcification was depressed at Maug, but not PNG. Whereas large (>4 m diam.) colonies of massive *Porites* were present at the Maug control site, and are evident in Fig. 3, the percentage cover (0.1%) was less than at low-CO_2 sites at PNG (10.7%). This suggests fundamental differences in the coral communities in the two regions, irrespective of acidified water, and may help to explain why the high-CO_2 communities are so different[23].

Whereas some coral species were found in higher abundances in close proximity to the vents (for example, *Leptastrea purpurea*) and are potentially stress tolerant[29], other species (for example, *Goniastrea edwardsi*) exhibited depressed abundances relative to the control site and could potentially be more sensitive to OA stress (Supplementary Table 7). Changes in community composition were also apparent among algae species (Supplementary Table 8) and the calcifying algae community was less abundant and less species-rich near the vent (Fig. 4 and Supplementary Fig. 4), supporting previous work[19].

As previously shown, CO_2-enrichment favours the proliferation of fleshy macroalgae[30]. We expect that the ecosystem shift, characterized by the dominance of fleshy macroalgae and lack of calcifying taxa near the high-p_{CO_2} site, is due in part to competition[12]. Different physiological responses to elevated p_{CO_2} disrupt and rearrange inter-specific competitive hierarchies[11]. For example, OA-enhanced algae production can indirectly inhibit coral growth through competition, mimicking the effects of direct OA-depressed coral calcification[31]. Similarly, OA can directly influence early life stages of corals[32], but high fleshy algae cover and perturbed crustose coralline algae (CCA) communities[33] can exaggerate this response by restricting coral recruitment. Finally, elevated p_{CO_2} could increase the ability of macroalgae to produce harmful allelochemicals or release dissolved organic carbon, which may further alter the microbial community and health of the coral holobiont[11].

This is the first study to report a shift from a coral to macroalgae-dominated ecosystem in a natural setting at pH conditions projected to occur by the end of the century. Although vent-associated reefs in PNG similarly exhibited elevated fleshy macroalgae and lower CCA cover, there was no significant difference in percentage coral cover at a pH of 7.8, owing to a higher prevalence of massive *Porites*[23]. By contrast, at Iwotorishima, OA-influenced reefs were dominated by soft versus hard corals[24]. One possible reason for the dominance of macroalgae at Maug is that the vent-induced OA gradient may be more stable than other sites owing to the relatively sheltered location inside a caldera (Fig. 1). At previously studied sites, periodic high winds[23] and tides[24] temporarily reduced the vent signal. Alternatively, the unique but unknown disturbance history (for example, bleaching, cyclones) of CNMI, versus high-latitude Iwotorishima and climatically favourable PNG, may increase the likelihood of state changes due to OA. For example, in the Galápagos, periodic temperature anomalies and upwelling-induced OA stress similar to that observed at Maug have been shown to result in reduced calcification of massive *Porites* and restricted reef development[15]. Furthermore, although the gas composition and environmental characteristics appeared similar at Maug, PNG and Iwotorishima, we cannot completely eliminate the possibility that other unquantified physical and chemical factors (for example, dissolved oxygen, nutrients) are correlated with volcanic CO_2 gradients. Increases in nutrients, both dissolved and particulate, can lead to algal dominance on reefs[31]. The reduced PAR near the vent was due to an increase in suspended particulate matter. These particulates may act as an unquantified source of nutrients associated with the seep that are acting in concert with high CO_2 to cause the community shift to macroalgal dominance. The interaction of high nutrients and CO_2 has been hypothesized to be a factor for why reefs disappear at higher pH values in the Galápagos (pH = 8.0), relative to PNG (pH = 7.7; ref. 15). The combination

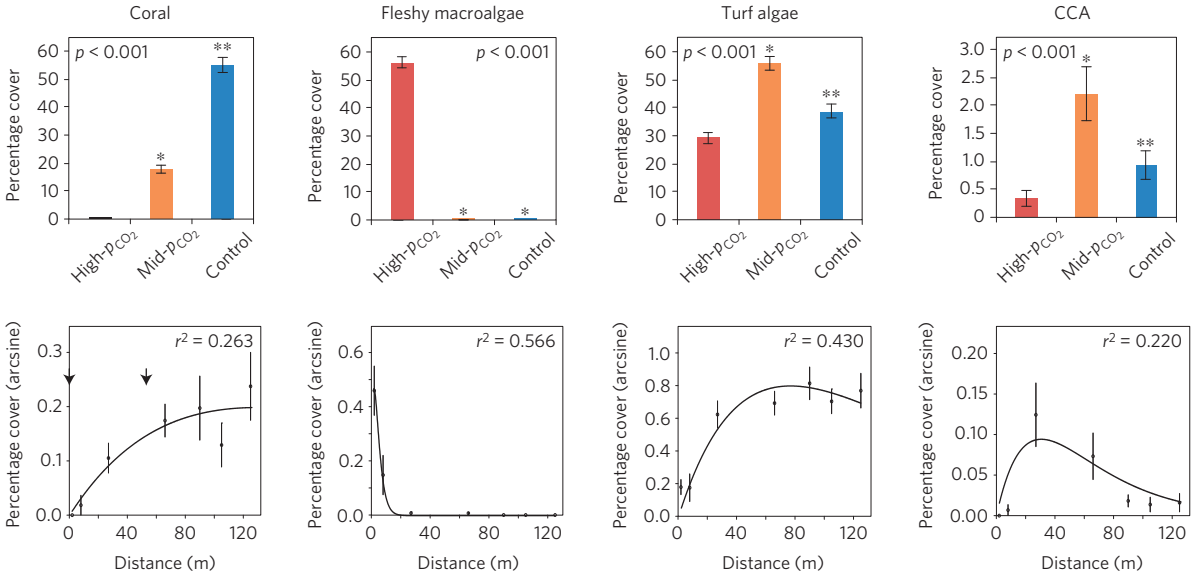

Figure 4 | The influence of vent proximity on the cover of coral reef taxa. Differences in benthic cover between high-p_{CO_2}, mid-p_{CO_2} and control sites (top, 100 photo quadrats per site) and regression of coral and algae percentage cover as a function of distance from the high-p_{CO_2} site (bottom, 11 quadrats per distance). Arrows in the coral regression panel denote locations of the high-p_{CO_2} and mid-p_{CO_2} sites. CCA is crustose coralline algae. Error bars are standard error of the mean. p and r^2 values given in the bar and the regression graphs, respectively. Values that do not share a symbol are significantly different. Percentage cover data are arcsine-transformed before analysis.

of elevated nutrients and high CO_2 could also play a role in the differences between Maug and the other reef seep sites.

In addition to physical and chemical differences, numerous ecological interactions (for example, competition, predation, herbivory) may be responsible for the unique OA-induced state shift observed at Maug. Although herbivores were present at the high-p_{CO_2} site, the dominant species of algae (*S. stipitatum*) is known from other localities to have low intracellular pH and is avoided by herbivores[34,35]. These factors may contribute to the proliferation of this species at the Maug site. Regardless of the mechanism, further research is needed to better understand what causes the different low-pH reef states that have been documented in this study, PNG, Japan and Palau.

Alteration of reef community composition at Maug due to elevated CO_2 does not bode well for the future of coral reefs worldwide as oceanic pH drops. Community shifts from coral to macroalgae dominance are occurring globally, and this trend is expected to continue given current climatic predictions[4]. Although the agents of coral mortality are numerous, the reefs at Maug are far-removed from localized anthropogenic stressors such as overfishing and land-based sources of pollution. Regardless, low seawater pH is correlated with a shift from coral-dominated to algae-dominated systems. Our results therefore suggest that OA can lead to a shift from coral to macroalgae dominance at pH values projected to occur by the end of the century.

Methods

Methods and any associated references are available in the online version of the paper.

Received 10 March 2015; accepted 15 July 2015;
published online 10 August 2015

References

1. Feely, R. A. *et al.* Impact of anthropogenic CO_2 on the $CaCO_3$ system in the oceans. *Science* **305,** 362–366 (2004).
2. Fabry, V. J., Seibel, B. A., Feely, R. A. & James, O. C. Impacts of ocean acidification on marine fauna and ecosystem processes. *ICES J. Mar. Sci.* **65,** 414–432 (2008).
3. Langdon, C. & Atkinson, M. Effect of elevated p_{CO_2} on photosynthesis and calcification of corals and interactions with seasonal change in temperature/irradiance and nutrient enrichment. *J. Geophys. Res.* **110,** C09S07 (2005).
4. Hoegh-Guldberg, O. *et al.* Coral reefs under rapid climate change and ocean acidification. *Science* **318,** 1737–1742 (2007).
5. Connell, S. D., Kroeker, K. J., Fabricius, K. E., Kline, D. I. & Russell, B. D. The other ocean acidification problem: CO_2 as a resource among competitors for ecosystem dominance. *Phil. Trans. R. Soc. B* **368,** 20120442 (2013).
6. Reaka-Kudla, M. L. in *Biodiversity II* (eds Reaka-Kudla, M. L., Wilson, D. E. & Wilson, E. O.) Ch. 7, 83–108 (Joseph Henry Press, 1997).
7. Moberg, F. & Folke, C. Ecolgoical goods and services of coral reef ecosystems. *Ecol. Econ.* **29,** 215–233 (1999).
8. Enochs, I. C. *et al.* Ocean acidification enhances the bioerosion of a common coral reef sponge: Implications for the persistence of the Florida Reef Tract. *Bull. Mar. Sci.* **91,** 271–291 (2015).
9. Eyre, B. D., Andersson, A. J. & Cyronak, T. Benthic coral reef calcium carbonate dissolution in an acidifying ocean. *Nature Clim. Change* **4,** 969–976 (2014).
10. Johnson, M. D., Price, N. N. & Smith, J. E. Contrasting effects of ocean acidification on tropical fleshy and calcareous algae. *PeerJ* **2,** e411 (2014).
11. Diaz-Pulido, G., Gouezo, M., Tilbrook, B., Dove, S. & Anthony, K. R. High CO_2 enhances the competitive strength of seaweeds over corals. *Ecol. Lett.* **14,** 156–162 (2011).
12. Kroeker, K. J., Micheli, F. & Gambi, M. C. Ocean acidification causes ecosystem shifts via altered competitive interactions. *Nature Clim. Change* **3,** 156–159 (2012).
13. Jokiel, P. L. *et al.* Ocean acidification and calcifying reef organisms: A mesocosm investigation. *Coral Reefs* **27,** 473–483 (2008).
14. Shaw, E. C., McNeil, B. I. & Tilbrook, B. Impacts of ocean acidification in naturally variable coral reef flat ecosystems. *J. Geophys. Res.* **117,** C03038 (2012).
15. Manzello, D. P. *et al.* Galápagos coral reef persistence after ENSO warming across an acidification gradient. *Geophys. Res. Lett.* **41,** 9001–9008 (2015).
16. Crook, E. D., Cohen, A. L., Rebolledo-Vieyra, M., Hernandez, L. & Paytan, A. Reduced calcification and lack of acclimatization by coral colonies growing in areas of persistent natural acidification. *Proc. Natl Acad. Sci. USA* **110,** 11044–11049 (2013).
17. Shamberger, K. E. F. *et al.* Diverse coral communities in naturally acidified waters of a Western Pacific reef. *Geophys. Res. Lett.* **41,** 499–504 (2014).
18. Martin, S. *et al.* Effects of naturally acidified seawater on seagrass calcareous epibionts. *Biol. Lett.* **4,** 689–692 (2008).
19. Hall-Spencer, J. M. *et al.* Volcanic carbon dioxide vents show ecosystem effects of ocean acidification. *Nature* **454,** 96–99 (2008).
20. Kroeker, K. J., Gambi, M. C. & Micheli, F. Community dynamics and ecosystem simplification in a high-CO_2 ocean. *Proc. Natl Acad. Sci. USA* **110,** 12721–12726 (2013).

21. Kerfahi, D. *et al.* Shallow water marine sediment bacterial community shifts along a natural CO_2 gradient in the Mediterranean Sea off Vulcano, Italy. *Microb. Ecol.* **67,** 819–828 (2014).
22. Milazzo, M. *et al.* Ocean acidification impairs vermetid reef recruitment. *Sci. Rep.* **4,** 1–7 (2014).
23. Fabricius, K. E. *et al.* Losers and winners in coral reefs acclimatized to elevated carbon dioxide concentrations. *Nature Clim. Change* **1,** 165–169 (2011).
24. Inoue, S., Kayanne, H., Yamamoto, S. & Kurihara, H. Spatial community shift from hard to soft corals in acidified water. *Nature Clim. Change* **3,** 683–687 (2013).
25. Marubini, F., Barnett, H., Langdon, C. & Atkinson, M. J. Dependence of calcification on light and carbonate ion concentration for the hermatypic coral *Porites compressa*. *Mar. Ecol. Prog. Ser.* **220,** 153–162 (2001).
26. Baker, A. C., Glynn, P. W. & Riegl, B. Climate change and coral reef bleaching: An ecological assessment of long-term impacts, recovery trends and future outlook. *Estuar. Coast. Shelf Sci.* **80,** 435–471 (2008).
27. Hurd, C. L. Water motion, marine macroalgal physiology, and production. *J. Phycol.* **36,** 453–472 (2000).
28. Iguchi, A. *et al.* Effects of acidified seawater on coral calcification and symbiotic algae on the massive coral *Porites australiensis*. *Mar. Environ. Res.* **73,** 32–36 (2012).
29. van Woesik, R., Sakai, K., Ganase, A. & Loya, Y. Revisiting the winners and the losers a decade after coral bleaching. *Mar. Ecol. Prog. Ser.* **434,** 67–76 (2011).
30. Johnson, V. R., Russell, B. D., Fabricius, K. E., Brownlee, C. & Hall-Spencer, J. M. Temperate and tropical brown macroalgae thrive, despite decalcification, along natural CO_2 gradients. *Glob. Change Biol.* **18,** 2792–2803 (2012).
31. McCook, L. J. Macroalgae, nutrients and phase shifts on coral reefs scientific issues and management consequences for the Great Barrier Reef. *Coral Reefs* **18,** 357–367 (1999).
32. Albright, R., Mason, B., Miller, M. & Langdon, C. Ocean acidification compromises recruitment success of the threatened Caribbean coral *Acropora palmata*. *Proc. Natl Acad. Sci. USA* **107,** 20400–20404 (2010).
33. Doropoulos, C., Ward, S., Diaz-Pulido, G., Hoegh-Guldberg, O. & Mumby, P. J. Ocean acidification reduces coral recruitment by disrupting intimate larval–algal settlement interactions. *Ecol. Lett.* **15,** 338–346 (2012).
34. Sasaki, H., Kataoka, H., Murakami, A. & Kawai, H. Inorganic ion compositions in brown algae, with special reference to sulfuric acid ion accumulations. *Hydrobiologia* **512,** 255–262 (2004).
35. Disalvo, L. H., Randall, J. E. & Cea, A. Stomach contents and feeding observations of some Easter Island fishes. *Atoll Res. Bull.* **548,** 1–22 (2007).

Acknowledgements

Funding was provided by NOAA's CRCP and OAP. We are grateful for the support and guidance of F. Rabauliman and F. Castro at BECQ/DCRM, M. Pangelinan and T. Miller at DFW, as well as J. Morgan, J. Tomczuk and D. Okano at NOAA. The crews of the Hi'Ialakai and Super Emerald provided logistic support. F. Forrestal and T. Dearg provided assistance with developing the manuscript.

Author contributions

I.C.E., D.P.M., E.M.D., G.K., R.O., L.J., C.Y., J.I., S.J., D.B., R.C. and N.N.P. assisted in study design and project planning. I.C.E., E.M.D., G.K., R.O., L.J., C.Y., J.I., C.B.E., M.D.F., S.J., D.B. and S.J.C. collected the data presented herein. I.C.E., D.P.M., E.M.D., G.K., R.O., L.J., J.I., C.B.E., M.D.F., L.V., S.J., D.B., S.J.C., R.C., T.B., Y.E. and N.N.P. worked on data analysis. I.C.E., D.P.M., E.M.D., G.K., R.O., L.J., C.Y., C.B.E., M.D.F., L.V. and N.N.P. contributed to manuscript preparation.

Additional information

Supplementary information is available in the online version of the paper. Reprints and permissions information is available online at www.nature.com/reprints. Correspondence and requests for materials should be addressed to I.C.E.

Competing financial interests

The authors declare no competing financial interests.

Methods

Study site. This study was conducted at Maug Island (20° 1′ N, 145° 13 E), in the northernmost region of the CNMI (Fig. 1). Initial investigation of the pH/CO_2 gradient was conducted with a pH probe (ROSS Ultra pH, Orion) and non-dispersive infrared CO_2 analyser (LI-820, LI-COR Biosciences) paired with a Global Positioning System (GPS). These data were used to inform subsequent chemical, environmental and biological sampling. For the purposes of this study, three sites were established along a gradient of vent influence. A high-p_{CO_2} site was located along the vent field/reef margin. An intermediate, mid-p_{CO_2} site was located roughly 50 m south of the vent, in an area dominated by reef framework and coral. Finally, an unaffected control site was located on the southern end of the island, roughly 1 km south of the research site. All were located at approximately nine metres depth, to control the influence of extraneous sources of variance during comparison.

Environmental data. To characterize the extent of carbonate chemistry alteration, 33 discrete water samples were collected in a grid pattern over the area influenced by the vent, covering both the high-p_{CO_2} and mid-p_{CO_2} sites. Water was collected from 20 cm below the water's surface using borosilicate glass bottles, which were immediately fixed with $HgCl_2$ and sealed. Temperature and salinity were recorded at the same depth using a handheld meter (EC300A, YSI) and sites were marked with a handheld GPS (GPSMAP 78S, Garmin). Water samples were collected in the same manner at the control site.

Samples were transported to NOAA's Atlantic Oceanographic and Meteorological Laboratories (AOML), where they were analysed for dissolved inorganic carbon (DIC) and total alkalinity (TA) using autotitrators (AS-C3 and AS-ALK2 respectively, Apollo SciTech). The carbonic acid system was solved using CO2SYS (ref. 36) with the dissociation constants of ref. 37 as refitted by ref. 38 and ref. 39 for boric acid. Carbonate chemistry parameters were plotted over the extent of the vent using ArcGIS (ESRI). An interpolated raster map was created from these points using the Spatial Analyst Toolbox and the inverse distance weighted (IDW) technique.

SeaFET pH loggers were deployed and recorded data every half hour at each of the three sites (control, mid-p_{CO_2}, high-p_{CO_2}). Data were collected from 19 May to 10 August 2014. Shorter-term diel oscillation in carbonate chemistry was investigated using discrete water samples collected every 6 h over a 48 h period from 11 August to 13 August 2014. Water was collected at each of the three study sites immediately above the benthos using a Niskin bottle, and then immediately transferred to borosilicate bottles while minimizing bubble formation and gas exchange. Samples were analysed with the same methodology used for spatial characterization.

Temperature loggers (HOBO Water Temp Pro v2, Onset) were deployed over the same period as the SeaFETs and were attached to stable platform bases approximately 10 cm above the benthos at the control, mid-p_{CO_2} and high-p_{CO_2} sites.

Light loggers (ECO-PAR, Wet Labs) were placed at each of the three sites and were programmed to record photosynthetically active radiation (PAR, 400–700 nm) every 30 min from 19 May to 9 August 2014. The instrument at the high-p_{CO_2} site failed immediately on deployment. The mid-p_{CO_2} and control site instruments were subsequently redeployed at the high-p_{CO_2} and control sites, collecting every 10 min from 10–13 August, to measure relative PAR levels. ECO-PAR instruments contain wipers that clean the sensor after each reading, and no drift was observed over the deployment period. We report daily PAR dose following ref. 40, where mean PAR over the period 10 am to 3 pm is multiplied by the total time of that period (5 h).

Two acoustic Doppler current profilers (ADCPs, Nortek Aquadopp) were deployed at the high-p_{CO_2} and control sites to measure current. The upward facing devices were turned over during a storm and stopped recording useable data on 4 July.

Vent gas was collected underwater using a conical collection cup connected to gas impermeable 1 l Tedlar sampling bags. Sealed bags were transported to Miami and subsequently analysed using gas chromatography (Varian CP3800 and HP 5890).

Biological data. Changes in benthic cover were investigated using photo quadrats and was conducted across two spatial scales: large-scale differences between the three instrumented high-p_{CO_2}, medium-p_{CO_2} and control sites, and fine-scale community shifts occurring outside the zone of active bubbling, expressed as a function of proximity to the high-p_{CO_2} site. For quantification of benthic cover among sites, high-resolution photomosaics were constructed following ref. 41. Mosaics were subsequently subsampled into 100 images per site and the benthic cover under 30 randomly located points were identified using the CPCe software package[42]. To examine changes in benthic cover with increasing distance from the area of active bubbling, East–West oriented transects, perpendicular to the CO_2 gradient, were placed at increasing distance from the vent. Photos were taken every 2 m along the 20-metre transect, and were subsequently analysed using CPCe (ref. 42), whereby 40 random points were overlaid over each image and identified.

Finer-level taxonomic identification of coral and algae can be difficult from photographs and community richness data were collected *in situ* using SCUBA. As with benthic cover, analysis was conducted across both large and small spatial scales. Immediately outside of the vent, six 15 m transects were placed, starting at ~5 m depth, and arranged perpendicular to the shore (East–West). Transects were spaced 10–20 m apart, incrementally further away from the vent site (North–South). Five 0.25 m^2 quadrats were placed haphazardly along each transect. All algae species within each quadrat were identified to the lowest reliable taxonomic level. Analysis of algae richness was conducted on all identified algae taxa (excluding turf algae), as well as on calcifying algae species, as shown in Supplementary Table 8. Turf algae is defined as the low-lying (<2 cm) community of small and juvenile algae species that are not taxonomically distinguishable *in situ*. Five additional 0.25 m^2 quadrats were used to quantify coral richness, as listed in Supplementary Table 7. Species-specific prevalences at each site were calculated as the proportion of richness quadrats containing each species, and 95% confidence intervals were calculated following ref. 43. For larger-scale site comparisons of community richness, near-vent data were grouped and compared against three additional transects placed at the control site.

Cores (5 cm diam. × 10 cm length) were taken from colonies of massive *Porites* sp. in close proximity to the instrumented mosaic sites using a pneumatic drill and SCUBA tank rig. Cores were slabbed parallel to the growth axis and scanned using microCT (Skyscan 1174, Bruker). Density was plotted versus distance and Coral XDS+ (ref. 44) was used to delineate yearly banding (peak–peak method), as well as to calculate extension, density and calcification rate.

Statistical analysis. Light was analysed using a *t*-test (2-tailed). Current and pH data were analysed using nonparametric Mann–Whitney and Kruskal–Wallis tests, respectively. Percentage cover data were arcsine-transformed[45] and analysed using general linear models (GLMs). Species richness data were $\log_e$-transformed and were analysed using *t*-tests (2-tailed). Transformation was unnecessary for coral core and calcification data, which were presented by year. Sample-specific averages over a five-year period (2009–2013) were compared between sites using GLMs. *Post hoc* pair-wise comparisons were conducted with Tukey's tests.

To investigate the effects of vent proximity on benthic community composition at the vent site, linear ($y = b_0 + b_1 x$), parabolic ($y = b_0 + b_1 x + b_2 x^2$), asymptotic ($y = b_0 + b_1 x^{-1}$) and Ricker models ($b_0 x e^{-b_1 x}$) were fitted to percentage coral cover data. Linear, parabolic and asymptotic models were fitted to coral, algae and calcifying algae community richness data. Goodness of fit was evaluated on statistical significance ($p < 0.05$), R^2, and Akaike's information criterion (AIC). Statistical analysis was conducted with the SPSS and GraphPad Prism software packages[46,47].

References

36. Program developed for CO_2 system calculations (ORNL/CDIAC, 1998).
37. Mehrbach, C., Culberson, C. H., Hawley, J. E. & Pytkowicz, R. M. Measurement of the apparent dissociation constants of carbonic acid in seawater at atmospheric pressure. *Limnol. Oceanogr.* **18,** 897–907 (1973).
38. Dickson, A. G. & Millero, F. J. A comparison of the equilibrium constants for the dissociation of carbonic acid in seawater media. *Deep-Sea Res.* **34,** 1733–1743 (1987).
39. Dickson, A. G. Thermodynamics of the dissociation of boric acid in synthetic seawater from 273.15 to 318.15 K. *Deep-Sea Res.* **37,** 755–766 (1990).
40. Manzello, D. *et al.* Remote monitoring of chlorophyll fluorescence in two reef corals during the 2005 bleaching event at Lee Stocking Island, Bahamas. *Coral Reefs* **28,** 209–214 (2009).
41. Gintert, B. *et al.* in *Proc. 11th Int Coral Reef Symp.* 577–581 (Nova Southeastern Univ., 2008).
42. Kohler, K. E. & Gill, S. M. Coral Point Count with Excel extensions (CPCe): A Visual Basic program for the determination of coral and substrate coverage using random point count methodology. *Comp. Geosci.* **32,** 1259–1269 (2006).
43. Newcombe, R. G. Two-sided confidence intervals for the single proportion: Comparison of seven methods. *Stat. Med.* **17,** 857–872 (1998).
44. Helmle, K., Kohler, K. & Dodge, R. *The Coral X-Radiograph Densitometry System: Coral XDS* (Nova Southeastern Univ., 2015); http://www.nova.edu/ocean/coralxds/index.html
45. Sokal, R. R. & Rohlf, F. J. *Biometry* (WH Freeman, 1981).
46. *IBM SPSS Statistics for Windows* (2013); http://www-01.ibm.com/software/analytics/spss
47. *GraphPad Prism* (2012); http://www.graphpad.com/scientific-software/prism